metals

MDPI

Article

The Effect of Thermal Cycling Treatments on the Thermal Stability and Mechanical Properties of a Ti-Based Bulk Metallic Glass Composite

Fan Bu, Jun Wang *, Liyuan Li, Hongchao Kou, Xiangyi Xue and Jinshan Li

State Key Laboratory of solidification processing, Northwestern Polytechnical University, Xi'an 710072, China; 18709251269@163.com (F.B.); liliyuan1943@126.com (L.L.); hchkou@nwpu.edu.cn (H.K.); xuexy@nwpu.edu.cn (X.X.); ljsh@nwpu.edu.cn (J.L.)

* Correspondence: nwpuwj@nwpu.edu.cn; Tel.: +86-29-8846-0568; Fax: +86-29-8846-0294

Academic Editor: Akihiko Hirata

Received: 12 September 2016; Accepted: 1 November 2016; Published: 10 November 2016

Abstract: The effect of thermal cycling treatments on the thermal stability and mechanical properties of a $Ti_{48}Zr_{20}Nb_{12}Cu_5Be_{15}$ bulk metallic glass composite (BMGC) has been investigated. Results show that moderate thermal cycles in a temperature range of −196 °C (cryogenic temperature, CT) to 25 °C (room temperature, RT) or annealing time at CT has not induced obvious changes of thermal stability and then it decreases slightly over critical thermal parameters. In addition, the dendritic second phases with a bcc structure are homogeneously embedded in the amorphous matrix; no visible changes are detected, which shows structural stability. Excellent mechanical properties as high as 1599 MPa yield strength and 34% plastic strain are obtained, and the yield strength and elastic modulus also increase gradually. The effect on the stability is analyzed quantitatively by crystallization kinetics and plastic-flow models, and indicates that the reduction of structural relaxation enthalpy, which is related to the degradation of spatial heterogeneity, reduces thermal stability but does not imperatively deteriorate the plasticity.

Keywords: BMGC; thermal stability; structure relaxation; mechanical property

1. Introduction

Compared with traditional crystals, bulk metallic glass (BMG) possesses high fracture strength, excellent wear and corrosion resistance, and great hardness thanks to the distinctive microstructures, which are needed for applications in many fields [1–3]. However, almost all BMGs exhibit catastrophic brittleness due to the limited deformation behavior of localized dominant shear bands [4]. To address this drawback, one can improve the plasticity by alloy optimization [5,6] or new technologies such as a mandrel winding method at room temperature [7] and thermal cycling treatment for rare-earth based amorphous alloys [8]. BMGs are also widely applied to fabricate in situ formed secondary ductile phase reinforced BMGCs [9–11]. Unfortunately, the glassy matrix is metastable and may transform spontaneously to a crystalline state. The ambient atmosphere affects the mobility of atoms greatly: when specimens are annealed at lower temperature (far below T_g), atoms may undergo structural relaxation [12,13] and some can slowly move to equilibrium positions, reaching a new metastable state. Structural relaxation always links to the mechanical properties of metallic glasses [7,14,15]; thermal stability, defined as a resistance to crystallization, is also relevant to β relaxation (a typical type of structural relaxation). For instance, Ichisubo et al. reported that ultrasonic annealing may accelerate the precipitation of the crystal phase and deteriorate the thermal stability [16].

Recently, the thermal stability and crystallization kinetics of a large amount of BMGs prepared using different manufacturing routes have been characterized [17–19]. If severe structural relaxation or

crystallization occurs, metallic glasses may lose strength and start aging. To circumvent this problem, many precautions have been taken to impede aging. Component optimization is efficient due to complex atomic interaction [20–22]. Attemperation is a simple and low-cost method that has been developed in many metallic alloy systems such as La-Ni-Al [8], Ti-Zr-Be-Al [23], Zr-Ti-Cu-Ni-Be [24], and Ni-Zr-Ti-Si [25]. However, hitherto, very limited studies have been performed on the thermal stability of BMGCs, so it is necessary to explore the optimal technological parameters to rejuvenate BMGCs; on the other hand, the aging mechanism also needs to be researched in depth.

Ti-based BMGCs attract interest because of their potential as structure materials [19,26–31]. $Ti_{48}Zr_{20}Nb_{12}Cu_5Be_{15}$ alloys possess greater plasticity and higher yield strength. For instance, Bai et al. focused on the quasi-static and dynamic deformation behavior at CT and an excellent cryogenic plasticity (totally 17.5%, at 5×10^{-4} s^{-1}) was observed under quasi-static deformation [19]. Li et al. report excellent CT mechanical properties as high as 2760 MPa fracture strength and 18.4% plastic strain due to the interaction between secondary phases and shear bands [26]. Li et al. prepared this alloy under a medium vacuum system by adding different contents of oxygen and nitrogen, which mainly affects the dendritic strength and enhances work-hardening behaviors [31]. However, few studies on thermal stability of this alloy have been published. The aim of this work is to investigate the effect of thermal cycling treatments on the thermal stability and mechanical properties of that system. In addition, the research can explore a new aging-resistant technology for Ti-based BMGCs and verify its feasibility.

2. Materials and Methods

2.1. Material Preparation

The ingots of $Ti_{48}Zr_{20}Nb_{12}Cu_5Be_{15}$ (at. %) BMGC were prepared by arc melting. The raw elements (the purity of Be was 99.5%; the rest were above 99.9%) were melted under a Ti-gettered purified argon atmosphere in a water-cooled copper crucible. The ingots were re-melted several times to ensure their chemical homogeneity; thereafter, they were injected into a water-cooled copper mold to form cylindrical rods 3 mm in diameter and 80 mm in length. The rods were cut to ensure they were 6 mm in length precisely (see Figure S1).

2.2. Thermal Cycling

A liquid nitrogen (LN) container with good insulation and a cryogenic thermometer with a temperature control accuracy of ± 1 °C were used for this thermal cycling treatment. First, the test rods were wound using special low-temperature-resistant wires and connected to the self-designed LN caps (Figure 1a), then the rods were sealed into quartz tubes, fully immersed in LN and timing systems started until the thermometer showed CT, after several minutes, and finally taken out in the vicinity of RT for 5 min, which is a thermal cycle. The same container cap was produced in order to reduce the volatilization of LN. The temperature variation diagram with time during a thermal cycle is shown in Figure 1b. In this part, we focus mainly on the effect of cycling times and annealing time in CT on the thermal stability.

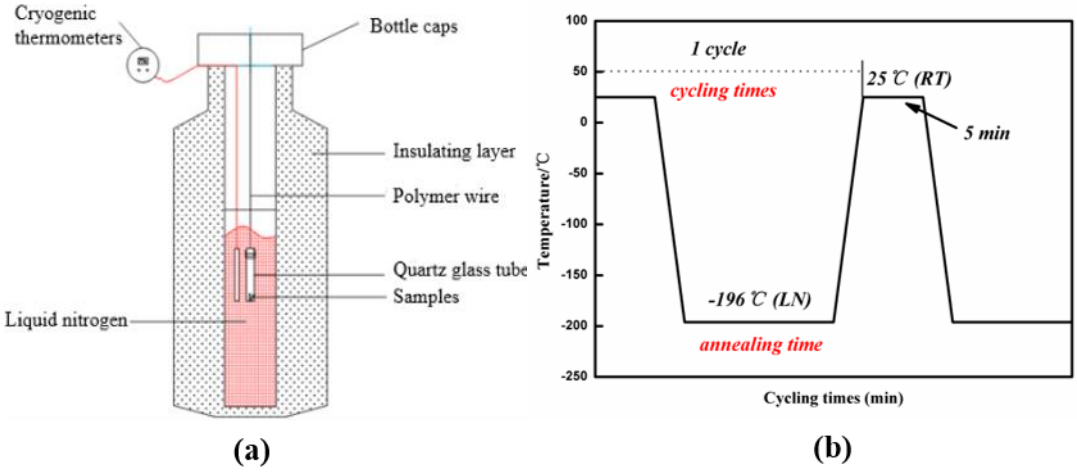

Figure 1. (**a**) Schematic of the experimental device and (**b**) the thermal cycling process diagram, where the red phrases are the experimental variables. (For details of the thermal parameters, see Table S1.)

2.3. Testing and Characterization

The different phases were detected by X-ray diffraction (XRD, DX-2700, Dandong Fangyuan Instrument Co. Ltd., Dandong, China) with Cu Kα radiation, the scanning angle was in the range of 20° to 90°, and 40 kV and 30 mA were chosen as the setup for the tube. The thermal stability was characterized by Differential Scanning Calorimeter (DSC, NEZTCH 402, Szerb, Germany), which could heating samples in an atmosphere of pure Argon with different heating rates of 10 °C/min, 20 °C/min and 40 °C/min so as to assess the thermal stability (determined by glass transition temperature T_g, onset crystallization temperature T_x, peak crystallization temperature T_p, and crystallization enthalpy ΔH). The BMGC microstructure, obtained after grounding and etching (HNO_3:HF:ethanol = 1:1:8), was observed with a Scanning Electron Microscope (SEM, TESCAN, Brno, Czech) performed on TESCAN VEGA3. Both sides of the rods were polished and placed parallel to each other and perpendicular to the loading axis. A uniaxial compressive mechanical test was operated using a MTS SANS CMT5105 machine (MTS Industrial Systems CO. LTD., Shenzhen, China) to evaluate the compressive yield strength and plasticity after different thermal cycling treatments under a strain rate of 10^{-4} s^{-1}.

3. Results and Discussion

3.1. Microstructure

Figure 2 shows the micro morphology of $Ti_{48}Zr_{20}Nb_{12}Cu_5Be_{15}$ BMGC with 0 and 20 rounds of thermal cycling, respectively. Compared with the SEM image of as-cast sample (0 cycle) by previous report [26,31], No obvious change has been detected and the dendrite secondary phases are homogeneously embedded in the amorphous matrix; the volume fraction of the secondary phases is 58% by estimating SEM images. Figure 3 depicts the XRD spectra of specimens with different thermal cycling; it demonstrates that the β-Ti (ZrNb) solid solution of BCC structure is added on the broad diffuse-scatter amorphous pattern. Apparently, a negligible difference in XRD spectra can be observed when compared with the as-cast sample, which is consistent with Figure 2a. Consequently, $Ti_{48}Zr_{20}Nb_{12}Cu_5Be_{15}$ BMGC could maintain structural stability under the studied thermal conditions.

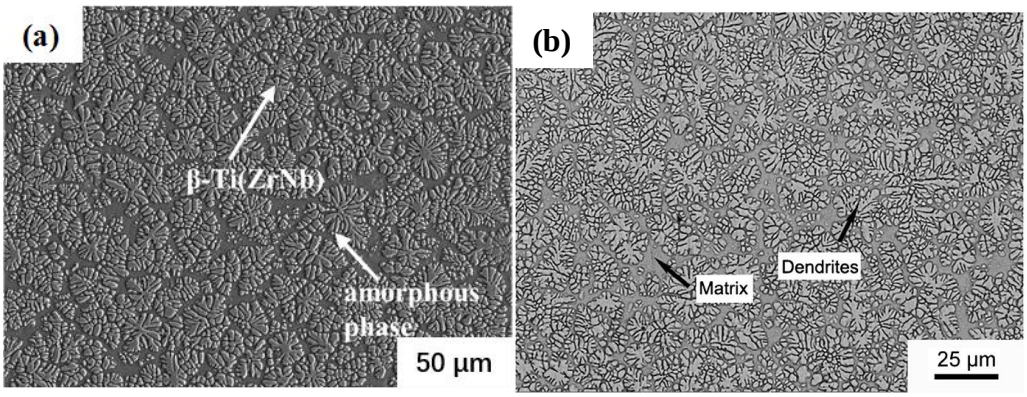

Figure 2. Microstructure morphologies (**a**) after 20 cycles of treatment and (**b**) without treatment [26].

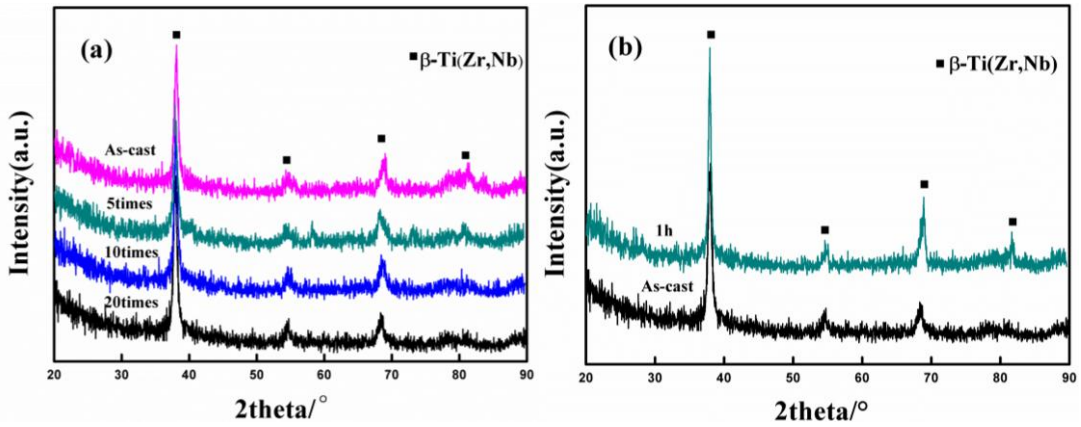

Figure 3. XRD patterns (**a**) after annealing for 1 min per cycle and (**b**) one cycle for different times in LN.

3.2. Thermal Stability

Figure 4a,b presents the DSC traces of the samples with a heating rate of 20 °C/min. As can be seen, all samples show a distinct glass transition and a supercooled liquid region (SLR) on DSC curves, i.e., small endothermic peaks occur at T_g near 380 °C (see Figure S2), implying that short-range atoms initially move to form many kinds of atomic clusters; subsequently, obvious exothermic peaks occur at T_x about 460 °C, showing a violent crystallization reaction. The original thermal parameters including T_g, T_x, ΔT (defined as $T_x - T_g$) and ΔH measured from DSC curves are summarized in Table S1. It is known that the values of T_g, T_x, and ΔT for different treated samples are quite similar, which indicates that $Ti_{48}Zr_{20}Nb_{12}Cu_5Be_{15}$ BMCC alloy and its supercooled liquid possess good thermal stability in our moderate thermal cycling environment. However, both a long annealing time in CT and excessive cycles (e.g., 106 rounds of thermal cycling or LN annealing one week) lead to a decrease of T_x and ΔT. As a result, the temperature interval of SLR shows a minimum value of 72 °C (a decrease of 11.1%, approximately), indicating a reinforced crystallization trend and deterioration of thermal stability. On the other hand, samples that undergo excessive thermal treatments have a lower thermal enthalpy of crystallization (ΔH) than that of an as-cast sample, showing that the system may release less energy and satisfy the ordered atomic arrangement more easily. Related studies [32,33] show strong contact between T_g and the yield strength $\sigma_{0.2}$, hence it is important to have a stable T_g to achieve mechanical stability.

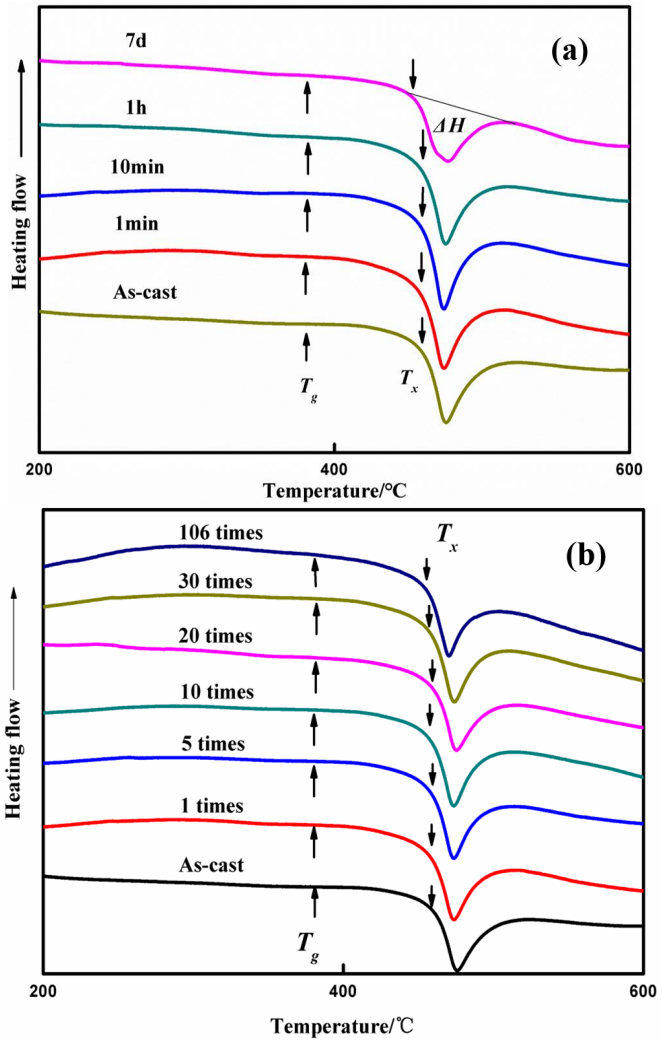

Figure 4. DSC traces after different experimental treatments: (**a**) single cycle and different annealing time in CT; (**b**) 1 min and different thermal cycles.

To further estimate the thermal stability of the $Ti_{48}Zr_{20}Nb_{12}Cu_5Be_{15}$ BMGC alloy, the reaction dynamics process can be characterized using the activation energies (ΔE), which can be expressed by the Kissinger and Ozawa methods [17,34,35]:

$$\ln\left(\frac{T^2}{\beta}\right) = \ln\left(\frac{\Delta E}{Rv_0}\right) + \frac{\Delta E}{RT} \quad (1)$$

$$\frac{d\ln\beta}{d\ln\left(\frac{1}{T}\right)} = -1.052\frac{\Delta E}{R} \quad (2)$$

$$k = v_0 \exp\left(-\frac{\Delta E}{RT}\right). \quad (3)$$

here ΔE is the characteristic activation energy; β is the heating rate; T is the different characteristic temperature including T_g, T_x, and T_p, which can be obtained from DSC curves recorded in non-isothermal mode using different heating rate; v_0 is the frequency factor, R is the gas constant; and k is the crystallization reaction rate. The Kissinger plots (see Figure S3), $\ln(T^2/\beta)$ vs. $1/T$, are established by linear fitting, hence the values of ΔE and v_0 can be easily calculated from Equations (1) and (2)

(the Kissinger and Ozawa methods, respectively). Moreover, the value of k can be obtained from Equation (3) (the Arrhenius method).

The thermal parameters of samples undergoing different annealing times with three different heating rates are summarized in Tables 1–3. (ΔE is a mean value calculated from Equations (1) and (2); all thermal kinetic parameters are listed in Tables S2–S4). Here the effect of different annealing time in LN was analyzed more deeply. It can be seen that ΔE and k have no obvious change near T_g and T_x between the as-cast and after 1 h treatment overall; when the glass transition starts, partial atoms absorb enough energy (mainly provided by the ambient temperature or severe plastic deformation) to become active and cross the energy barrier more easily, thus facilitating a crystallization reaction. The higher ΔE is, the more difficult it is for atoms to start transformation. Consequently, this system has great thermal stability owing to its wide SIRs and impervious ΔE. However, the glass transition activation energy E_g decreases from 143 kJ/mol (as-cast) to 128 kJ/mol (after one week, a reduction of 9.8%), indicating an increasing formation trend of SLR and the glassy matrix becoming fragile. A hypothesis is that visible changes may be detected when samples are annealed in LN more than one week.

Table 1. The characteristic temperatures, activation energy, and crystallization constant of as-cast.

Temperature	Scanning Rate (°C/min)			ΔE (kJ/mol)	(s^{-1})	k (s^{-1}) (20 °C/min)
	10	20	40			
T_g (°C)	366 ± 1	381 ± 2	398 ± 1	143 ± 3	2.32×10^{11}	
T_x (°C)	442 ± 1	459 ± 1	475 ± 1	176 ± 2	3.09×10^{12}	0.81
T_p (°C)	462 ± 1	475 ± 1	489 ± 2	227 ± 3	7.81×10^{15}	0.98
ΔT (°C)	76 ± 1	78 ± 1	77 ± 1			

Table 2. The characteristic temperatures, activation energy, and crystallization constant after 1 h.

Temperature	Scanning Rate (°C/min)			ΔE (kJ/mol)	(s^{-1})	k (s^{-1}) (20 °C/min)
	10	20	40			
T_g (°C)	367 ± 1	381 ± 1	399 ± 1	145 ± 2	3.03×10^{11}	
T_x (°C)	443 ± 2	460 ± 1	475 ± 2	183 ± 1	3.43×10^{12}	0.82
T_p (°C)	460 ± 1	475 ± 1	488 ± 3	217 ± 2	1.56×10^{15}	1.00
ΔT (°C)	76 ± 1	79 ± 1	76 ± 1			

Table 3. The characteristic temperatures, activation energy, and crystallization constant after one week.

Temperature	Scanning Rate (°C/min)			ΔE (kJ/mol)	(s^{-1})	k (s^{-1}) (20 °C/min)
	20	30	40			
T_g (°C)	381 ± 1	391 ± 1	399 ± 2	128 ± 2	6.30×10^{10}	
T_x (°C)	453 ± 1	462 ± 2	469 ± 2	184 ± 2	1.43×10^{12}	0.11
T_p (°C)	477 ± 1	481 ± 2	485 ± 1	377 ± 4	3.06×10^{26}	1.64
ΔT (°C)	72 ± 1	71 ± 1	70 ± 1			

Figure 5 denotes the temperature dependence of k. As we can see, all the curves show that the value of k increases monotonically with the improved temperature. Moreover, the values of k become larger and increase more dramatically near T_g after one week of treatment, illustrating that this sample is more easily crystallized. In addition, the crystallization behavior near T_x after different treatment changes a little and the effect is negligible. It is known that a slight structural relaxation occurs when amorphous alloys are in a cryogenic environment; meanwhile, the distance between short-ordered clusters may change, though they are usually 1–2 nm in magnitude [36,37]. A reasonable annealing process can relieve internal stresses previously existent in the metal; therefore, atomic arrangement

tends to become ordered and homogeneous. In addition, the annealing process provides enough time for atoms to diffuse. As a consequence, the types and scales of amorphous orders increase gradually with the annealing time, all of which can contribute to crystallization and a lower thermal stability occurring naturally. The characteristic parameters of the 1-h treated sample show nearly no change, which further proves that the thermal cycling treatments' function is not visible and they do not deteriorate the high thermal stability.

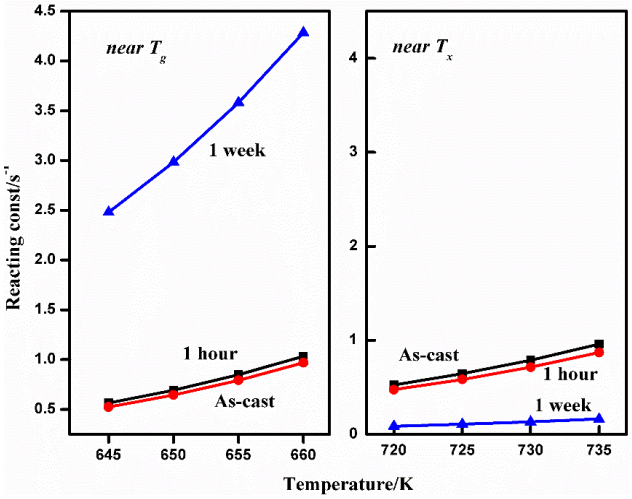

Figure 5. *k*–*T* curves of alloys with different annealing times in CT.

3.3. Mechanical Properties

Figure 6 displays the different thermal cycling parameters' dependence on Young's Modulus *E*, plastic strain ε, and yield strength $\sigma_{0.2}$, respectively. It can be clearly seen that ε remains stable (~34%), indicating that the deformation behavior of the shear band is not sensitive to this technology. In addition, *E* and $\sigma_{0.2}$ clearly increase after longer treatment. For instance, at a strain rate of 10^{-4} s^{-1}, the as-cast composite yields at about 1358 MPa and then follows a 34% plastic deformation until fracture at 2610 MPa, which is comparable to other studies [28,31]. However, after 1 h treatment, yield emerges at about 1590 MPa (with an enhancement of 13.7%) and the glassy matrix seems to become harder (for details about mechanical parameters, see Figures S4 and S5 and Tables S5 and S6).

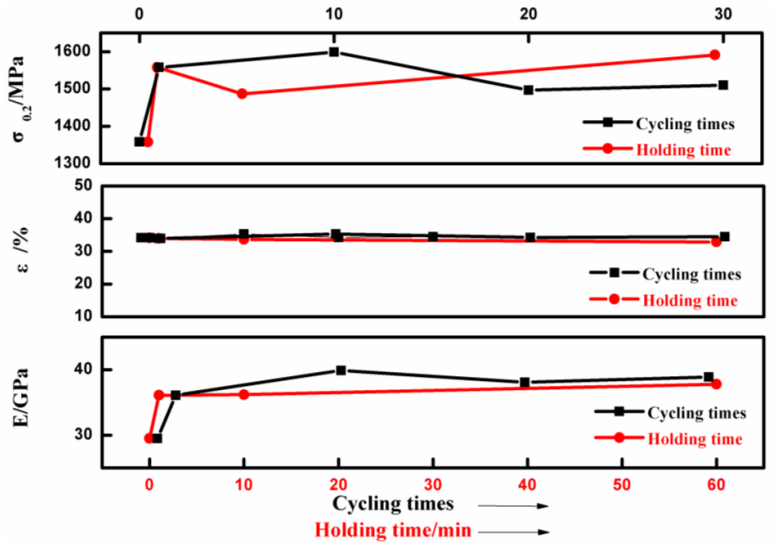

Figure 6. The summarized parameters of *E*, ε, and $\sigma_{0.2}$ with different cryogenic cycling treatments.

Although the origin of the slightly higher mechanical properties of the $Ti_{48}Zr_{20}Nb_{12}Cu_5Be_{15}$ BMGC with thermal cycling remains unclear, we mainly discuss the possibility of a free-volume and released strain effect; for most composites, they all observe the rule of mixture [38]:

$$\sigma_{comp} = \varphi_c \sigma_c + \varphi_g \sigma_g \tag{4}$$

where σ_{comp}, σ_c, and σ_g are the yield strength of BMCs, β-Ti phases, and glassy matrixes, respectively. φ is the fraction volume. This treatment mainly affects the amorphous phase through a slight relaxation. The crystal phase shown in Figure 2 is quite stable, so the total enhanced σ_{comp} may attribute to the improvement of σ_g, which can be expressed as Equation (5) [39]:

$$\sigma_y \approx 50 \frac{T_g - T_0}{V}, \tag{5}$$

where σ_g is the yield strength of the amorphous phase, V is the molar volume, and T_0 is the RT in compressive analysis. T_g and T_0 can be regarded as constants that are consistent with the thermal stability, so σ_g keeps constant theoretically; the fluctuation of data may be ascribed to slight structural relaxation and spatial heterogeneity, but actually the atoms are arranged in a compact and orderly manner, forming many clusters, which shows a reduction of φ_c and an increase of φ_g in nanoscales, resulting in an enhanced total yield strength ($\sigma_c < \sigma_g$) [36]. The amorphous atoms become stiffer after structural relaxation and the interaction force increases, hence the Young's modulus increases naturally.

Figure 7 shows an enlarged view of the glass transition regime of the DSC curve of the $Ti_{48}Zr_{20}Nb_{12}Cu_5Be_{15}$ BMGC after different numbers of cycles. A visible change in the exothermic event prior to T_g can be noticed. It has been well documented that exothermic event prior to T_g is related to structural relaxation of the metallic glass, which can be regarded as the result of the annihilation of free volume (ΔV_f) [40]. The reduction of ΔV_f can certainly decrease the average atomic distance and thus less energy is needed for structural relaxation, and structural relaxation enthalpy (ΔH_0) is proportional to ΔV_f [41]. With the increasing cycles, the value of ΔH_0 are 0.251 w/g, 0.211 w/g, 0.110 w/g, 0.123 w/g, 0.265 w/g, 0.066 w/g, and 0.091 w/g, respectively (see Table S7). Within experimental error, the structural relaxation enthalpy of this BMGC system has been decreased with the increment of thermal cycles N, indicating a reduction of ΔV_f, which may increase the elastic modulus and the resistance to the plastic deformation. The details will be discussed later.

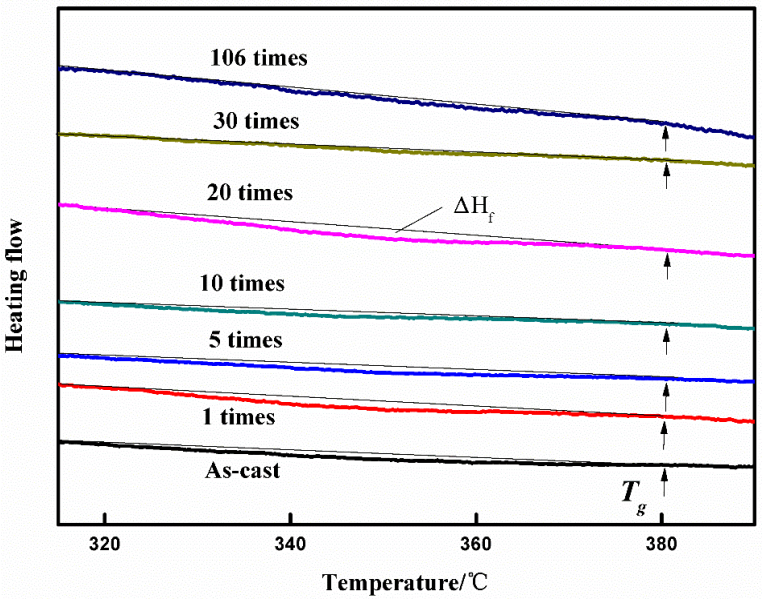

Figure 7. Enlarged image of the DSC scanning curves at low temperatures (arrows indicate T_g).

3.4. The Relationship between β Relaxation and Macro Properties

Ketov et al. found an eligible novelty of enhanced plasticity and hardness within La-based MGs after several cryogenic cycles, and observed a previously undetected microstructure [22]. However, for our Ti-based MGCs, this makes no obvious change in the macroscopic properties. One possible reason is as follows:

(1) β-relaxation is important in many properties of MGs [1–7,14,15], and is usually intensively affected both by ambient temperature and atoms' interaction: for most metallic glasses, such as La-based [4,5,7,14,22,38], Cu-based [38], Zr-based [34,38,41], and Pd-based [42], if the annealing temperature is higher than (0.6–0.8) T_g a more distinctive β peak (usually comparable with a loss modulus) can be detected, i.e., La-based MG is a better candidate because of its low T_g. In our system, thermal parameters T_g (~380 °C) and T_x (~460 °C) are determined, which is consistent with previous studies [31,33]; therefore, the estimating annealing temperature should be higher than RT to capture an obvious β-relaxation. So it is attractive to reach higher annealing temperatures when cycling.

(2) The thermal cycles also make a contribution to β relaxation. For example, Ketov et al. use technology to regulate spatial non-affine thermal strain and behaviors of "defects", and rejuvenation was mentioned [22]. For Ti-based BMGCs, the brittleness is effectively impeded by a secondary β-Ti phase with lower elastic stiffness and higher CTE [28–30]. β-Ti Crystalline phase is less effected due to their lower energy than that of amorphous matrixes thermodynamically, hence the behavior of amorphous matrixes during thermal cycles is more attractive. Wang et al. [32–34,38,43,44] established a relationship between the plasticity of MGs and β-relaxation using the flow-unit (FU) and shear-transition-zone (STZ) model. In our system, the effect of β-relaxation on the shear band's propagation and movement is trivial compared with that of crystalline phases, resulting in a nearly unchangeable plasticity; this proves that our Ti-based BMGCs have great mechanical and microstructure stability (see Figures 2 and 3).

What is more, the thermal cycling treatment may function in the nanoscale area by structural relaxation [36,37] and a degradation of spatial heterogeneity [43,44] induced by a released thermal strain. The possible reason is that annealing at a cryogenic temperature freezes the atom's movement and maintains great spatial heterogeneity, and the characteristic length of spatial heterogeneity increases over time. When the specimens are in RT, a low-temperature β relaxation occurs, leading to a decreased high-energy dissipation domain and the microstructure of metallic glass becoming more uniform; these effects can be more obvious as the annealing time increases. Generally, enhanced Young's modulus and yield strength (see Figure 6) are mainly ascribed to the loss of STZ and a uniform glass matrix [43,45,46]; in addition, many secondary phases provide a site for the absorption of amorphous atoms, thus there is more time to cross the energy barrier and reduced relaxation enthalpy is observed (see Figures 5 and 7). Therefore, T_x has a tendency to decrease over time during annealing (see Figure 4). The cycling time has a similar effect on thermal stability: with increasing cycles, the stress near the vicinity of interfaces between MGs and dendritic arms is released, which is also responsible for a dissipation of FU and STZ, i.e., the decreased relaxation enthalpy is actually due to the degradation of spatial heterogeneity [43,45].

Nevertheless, as for most metallic glass composites, thermal cycling treatments have the side effects of improving thermal stability: the boundaries of secondary phases, acting as barriers, absorb considerable internal stresses and block the diffusion routes; similarly, low temperature also decelerates the velocity of atoms. On the other hand, severe structural relaxation does harm to amorphous properties. These two factors are equally essential but contradictory; as a result, the effect on thermal stability is opposite, so there is a local balance when treated moderately. However, with the increasing cycles or annealing time in LN, thermal stability is mainly dominated by structural relaxation and a great reduction in residual stress; hence, a slight decrease in thermal stability occurs at the end.

However, hitherto, there have been few reports about thermal stability and its relaxation behavior related to BMGCs. Here we apply a new technology to Ti-based BMGCs and further systematic research into the effect of relaxation on BMGCs must continue. At present, thermal cycling treatment can also have a slight effect on the mechanical properties of Ti-based amorphous composites.

4. Conclusions

In the present work, $Ti_{48}Zr_{20}Nb_{12}Cu_5Be_{15}$ BMGC was prepared by arc-melting and copper casting methods, and the effects of thermal cycling on the thermal stability and mechanical properties of the specimens were investigated. The following conclusions are highlighted:

(1) Generally, the $Ti_{48}Zr_{20}Nb_{12}Cu_5Be_{15}$ BMGC system possesses great thermal stability (ΔT = 78 °C) and good plasticity (over 30%) in the present experimental conditions. With increasing cycles or annealing time in LN (e.g., one week or 106 cycles), thermal stability is mainly dominated by a slight β relaxation and great reduction in residual stress, so a slight decrease of thermal stability occurs by the end.

(2) The elastic modulus and yield strength increase a little because of the relaxation after treatment. The maximum $\sigma_{0.2}$ is 1599 MPa. No embrittlement evidence has been observed despite the decreased ΔH_0 of the BMGC. This indicates that the reduction of structural relaxation enthalpy, which is related to the degradation of spatial heterogeneity, does not necessarily result in embrittlement.

(3) $Ti_{48}Zr_{20}Nb_{12}Cu_5Be_{15}$ BMGC can keep great structural stability and no obvious change of microstructure can be detected after XRD and SEM analysis, indicating that the cryogenic treatment has a negligible effect on the phase distribution.

Supplementary Materials: The following are available online at www.mdpi.com/2075-4071/6/11/274/s1. Figure S1: Casting rods prepared by arc melting and cooper mold suck cast, Figure S2: Enlarged DSC curves of Figure 4a (a) as-cast and (b) 1 week, (c) 1 week with different heat rate, Figure S3: ln(T2/β) vs. 1/T. the activation energy near T_g, T_x and T_p with different cryogenic cycling treatment, Figure S4: Stress-strain curves after 1-cycle treatment with different annealing time, Figure S5: Stress-strain curves after 1-min treatment with different cycle, Table S1: Thermal parameters determined from different thermal cycling treatments (20 °C/min), Table S2: All thermal kinetic parameters near glass transition temperature, Table S3: All thermal kinetic parameters near beginning crystallization temperature, Table S4: The activation energy after different treatment, Table S5: Mechanical parameters after 1-min treatment with different cycles, Table S6: Mechanical parameters after 1-cycle treatment after different annealing time, Table S7: The heat release ΔH after different treatment.

Acknowledgments: This work was supported by specialized research funds for doctoral program of higher education (20136102120007), the fund of the State Key Laboratory of Solidification Processing in NWPU (No. 103-QP-2014), and the Fundamental Research Funds for the Central Universities (No. 3102015ZY085).

Author Contributions: J.W. and X.Y.X. conceived and designed the experiments; F.B. and L.Y.L. performed the experiments; J.W. and F.B. analyzed the data; H.C.K. and J.S.L. contributed reagents/materials/analysis tools; F.B. wrote the paper.

Conflicts of Interest: The authors declare no conflict of interest.

References

1. Inoue, A. Recent development and application products of bulk glassy alloys. *Acta Mater.* **2011**, *59*, 2243–2267. [CrossRef]
2. Trexler, M.M.; Thadhani, N.N. Mechanical properties of bulk metallic glasses. *Prog. Mater. Sci.* **2010**, *55*, 759–839. [CrossRef]
3. Inoue, A. Stabilization of metallic supercooled liquid and bulk amorphous alloys. *Acta Mater.* **2000**, *48*, 279–306. [CrossRef]
4. Xing, L.Q.; Li, Y.; Ramesh, K.T.; Li, J.; Hufnagel, T.C. Enhanced plastic strain in Zr-based bulk amorphous alloys. *Phys. Rev. B* **2001**, *64*, 607–611. [CrossRef]
5. Zhang, B.; Zhao, D.Q.; Pan, M.X.; Wang, W.H.; Greer, A.L. Amorphous metallic plastic. *Phys. Rev. Lett.* **2005**, *94*, 205502. [CrossRef] [PubMed]

6. Liu, Y.H.; Wang, G.; Wang, R.J.; Zhao, D.Q.; Pan, M.X.; Wang, W.H. Super plastic bulk metallic glasses at room temperature. *Science* **2007**, *315*, 1385–1388. [CrossRef] [PubMed]
7. Lu, Z.; Jiao, W.; Wang, W.H.; Bai, H.Y. Flow unit perspective on room temperature homogeneous plastic deformation in metallic glasses. *Phys. Rev. Lett.* **2014**, *113*, 045501. [CrossRef] [PubMed]
8. Zhu, S.L.; Wang, X.M.; Qin, F.X.; Inoue, A. A new Ti-based bulk glassy alloy with potential for biomedical application. *Mater. Sci. Eng. A* **2007**, *459*, 233–237. [CrossRef]
9. Hays, C.C.; Kim, C.P.; Johnson, W.L. Microstructure controlled shear band pattern formation and enhanced plasticity of bulk metallic glasses containing in situ formed ductile phase dendrite dispersions. *Phys. Rev. Lett.* **2000**, *84*, 2901–2904. [CrossRef] [PubMed]
10. Inoue, A.; Zhang, W.; Tsurui, T.; Yavari, A.R.; Greer, A.L. Unusual room-temperature compressive plasticity in nanocrystal-toughened bulk copper-zirconium glass. *Philos. Mag. Lett.* **2005**, *85*, 221–237. [CrossRef]
11. Zhu, Z.; Zhang, H.; Hu, Z.; Zhang, W.; Inoue, A. Ta-particulate reinforced Zr-based bulk metallic glass matrix composite with tensile plasticity. *Scr. Mater.* **2010**, *62*, 278–281. [CrossRef]
12. Schuh, C.A.; Hufnagel, T.C.; Ramamurty, U. Mechanical behavior of amorphous alloys. *Acta Mater.* **2007**, *55*, 4067–4109. [CrossRef]
13. Inoue, A.; Nishiyama, N.; Amiya, K.; Zhang, T.; Masumoto, T. Ti-based amorphous alloys with a wide supercooled liquid region. *Mater. Lett.* **1994**, *19*, 131–135. [CrossRef]
14. Yu, H.B.; Shen, X.; Wang, Z.; Bai, H.Y. Tensile plasticity in metallic glasses with pronounced β relaxations. *Phys. Rev. Lett.* **2012**, *108*, 140–144. [CrossRef] [PubMed]
15. Yu, H.B. Relating activation of shear transformation zones to β relaxations in metallic glasses. *Phys. Rev. B* **2010**, *81*, 235–246. [CrossRef]
16. Ichisubo, T.; Matsubara, E.; Yamamoto, T.; Chen, H.S.; Nishiyama, N.; Saida, J.; Anazawa, K. Microstructure of fragile metallic glasses inferred from ultrasound-accelerated crystallization in Pd-based metallic glasses. *Phys. Rev. Lett.* **2005**, *95*, 245501. [CrossRef] [PubMed]
17. Zhang, L.C.; Xu, J.; Eckert, J. Thermal stability and crystallization kinetics of mechanically alloyed TiC/Ti-based metallic glass matrix composite. *J. Appl. Phys.* **2006**, *100*, 033514. [CrossRef]
18. Datta, M.K.; Chou, D.T.; Hong, D.; Saha, P.; Chung, S.J.; Lee, B.; Sirinterlikci, A.; Ramanathan, M.; Roy, A.; Kumta, P.N. Structure and thermal stability of biodegradable Mg-Zn-Ca based amorphous alloys synthesized by mechanical alloying. *Mater. Sci. Eng. B* **2011**, *176*, 1637–1643. [CrossRef]
19. Bai, J.; Kou, H.C.; Wang, J.; Li, J.S.; Hu, R. Strain rate response of a Ti-based metallic glass composite at cryogenic temperature. *Mater. Lett.* **2014**, *117*, 228–230. [CrossRef]
20. Wu, X.Q.; Wang, H.L.; Lin, J.G. Effects of Sn content on thermal stability and mechanical properties of the $Ti_{60}Zr_{10}Ta_{15}Si_{15}$ amorphous alloy for biomedical use. *Mater. Des.* **2014**, *63*, 345–348. [CrossRef]
21. Li, X.; Bian, X.; Hu, L.; Wu, Y.; Zhang, J. Effect of microalloying on glass formation and thermal stability of Cu–Pr-based amorphous alloys. *J. Alloy. Compd.* **2007**, *439*, 87–90. [CrossRef]
22. Ketov, S.V.; Sun, Y.H.; Nachum, S.; Lu, Z.; Checchi, A.; Beraldin, A.R.; Bai, H.Y.; Wang, W.H.; Luzgin, D.V.L.; Carpenter, M.A.; et al. Rejuvenation of metallic glasses by nonaffine thermal strain. *Nature* **2015**, *524*, 200–203. [CrossRef] [PubMed]
23. Wang, X.; Shao, Y.; Gong, P.; Yao, K.F. The effect of simulated thermal cycling on thermal and mechanical stability of a Ti-based bulk metallic glass. *J. Alloy. Compd.* **2013**, *575*, 449–454. [CrossRef]
24. Wang, X.; Shao, Y.; Gong, P.; Yao, K.F. Effect of thermal cycling on the mechanical properties of $Zr_{41}Ti_{14}Cu_{12.5}Ni_{10}Be_{22.5}$ alloy. *Sci. China Phys. Mech. Astron.* **2012**, *55*, 2357–2361. [CrossRef]
25. Lee, J.K.; Bae, D.H.; Kim, W.T.; Kim, D.H. Effect of liquid temperature on thermal stability and crystallization behavior of Ni-based amorphous alloys. *Mater. Sci. Eng. A* **2004**, *375–377*, 332–335. [CrossRef]
26. Li, J.; Bai, J.; Wang, J.; Kou, H.; Hu, R.; Fu, H. Deformation behavior of a Ti-based bulk metallic glass composite with excellent cryogenic mechanical properties. *Mater. Des.* **2014**, *53*, 737–740. [CrossRef]
27. Cui, J.; Li, J.S.; Wang, J.; Kou, H.C. Microstructure Evolution and Mechanical Properties of a Ti-Based Bulk Metallic Glass Composite. *J. Mater. Eng. Perform.* **2015**, *24*, 2354–2358. [CrossRef]
28. Bai, J. Deformation Micro mechanisms of a Ti-Based Metallic Glass Composite with Excellent Mechanical Properties. *Mater. Sci. Forum* **2013**, *745–746*, 809–814. [CrossRef]
29. Park, J.M.; Jayaraj, J.; Kim, D.H.; Mattern, N.; Wang, G.; Eckert, J. Tailoring of in situ Ti-based bulk glassy matrix composites with high mechanical performance. *Intermetallic* **2010**, *18*, 1908–1911. [CrossRef]

30. Hofmann, D.C.; Johnson, W.L. Development of tough, low-density titanium-based bulk metallic glass matrix composites with tensile ductility. *Proc. Natl. Acad. Sci. USA* **2008**, *105*, 20136–20140. [CrossRef] [PubMed]
31. Li, L.; Kou, H.; Wang, J.; Li, J.; Hu, R. Enhanced mechanical properties of Ti-based metallic glass composites prepared under medium vacuum system. *J. Non-Cryst. Solids* **2015**, *413*, 15–19. [CrossRef]
32. Wang, W.H. Correlations between elastic moduli and properties in bulk metallic glasses. *J. Appl. Phys.* **2006**, *99*, 093506. [CrossRef]
33. Wang, W.H. Correlation between relaxations and plastic deformation, and elastic model of flow in metallic glasses and glass-forming liquids. *J. Appl. Phys.* **2011**, *110*, 053521. [CrossRef]
34. Kissinger, H.E. Reaction kinetics in differential thermal analysis. *Anal. Chem.* **2002**, *29*, 1702–1706. [CrossRef]
35. Lad, K.N.; Savalia, R.T.; Pratap, A.; Dey, G.K.; Banerjee, S. Isokinetic and isoconversional study of crystallization kinetics of a Zr-based metallic glass. *Thermochim. Acta* **2008**, *473*, 74–80. [CrossRef]
36. Jiang, W.H.; Liu, F.X.; Wang, Y.D.; Zhang, H.F.; Choo, H.; Liaw, P.K. Comparison of mechanical behavior between bulk and ribbon Cu-based metallic glasses. *Mater. Sci. Eng. A* **2006**, *430*, 350–354. [CrossRef]
37. Kim, S.J.; Hwang, S.W.; Yoon, C.S.; Kim, C.K. Structure and magnetic properties of thermally annealed Fe73Pt5B10Si12 amorphous metallic alloy. *Mater. Sci. Eng. B* **2004**, *108*, 266–270. [CrossRef]
38. Gargarella, P.; Pauly, S.; Khoshkhoo, M.S.; Kühn, U.; Eckert, J. Phase formation and mechanical properties of Ti-Cu-Ni-Zr bulk metallic glass composites. *Acta Mater.* **2014**, *65*, 259–269. [CrossRef]
39. Yang, B.; Liu, C.T.; Nieh, T.G. Unified equation for the strength of bulk metallic glasses. *Appl. Phys. Lett.* **2006**, *88*, 221911. [CrossRef]
40. Cohen, M.H. Free-volume model of the amorphous phase: Glass transition. *J. Chem. Phys.* **1961**, *34*, 120–125.
41. Slipenyuk, A.; Eckert, J. Correlation between enthalpy change and free volume reduction during structural relaxation of $Zr_{55}Cu_{30}Al_{10}Ni_5$, metallic glass. *Scr. Mater.* **2004**, *50*, 39–44. [CrossRef]
42. Meyer, A.; Busch, R.; Schober, H. Time-Temperature Superposition of Structural Relaxation in a Viscous Metallic Liquid. *Phys. Rev. Lett.* **1999**, *83*, 5027–5029. [CrossRef]
43. Zhu, F.; Nguyen, H.K.; Song, S.X.; Aji, D.P.B.; Hirata, A.; Wang, H.; Nakajima, K.; Chen, M.W. Intrinsic correlation between β-relaxation and spatial heterogeneity in a metallic glass. *Nat. Commun.* **2016**. [CrossRef] [PubMed]
44. Wang, W.H.; Yang, Y.; Nieh, T.G.; Liu, C.T. On the source of plastic flow in metallic glasses: Concepts and models. *Intermetallics* **2015**, *67*, 81–86. [CrossRef]
45. Wang, Z.; Wen, P.; Huo, L.S.; Bai, H.Y.; Wang, W.H. Signature of viscous flow units in apparent elastic regime of metallic glasses. *Appl. Phys. Lett.* **2012**, *101*, 121906. [CrossRef]
46. Huo, L.S.; Zeng, J.F.; Wang, W.H.; Liu, C.T.; Yang, Y. The dependence of shear modulus on dynamic relaxation and evolution of local structural heterogeneity in a metallic glass. *Acta Mater.* **2013**, *61*, 4329–4338. [CrossRef]

© 2016 by the authors; licensee MDPI, Basel, Switzerland. This article is an open access article distributed under the terms and conditions of the Creative Commons Attribution (CC-BY) license (http://creativecommons.org/licenses/by/4.0/).